ANTHROPOLOGY

# Wintertime stress, nursing, and lead exposure in Neanderthal children

**Tanya M. Smith[1]*†, Christine Austin[2†], Daniel R. Green[3,4†], Renaud Joannes-Boyau[5†], Shara Bailey[6], Dani Dumitriu[2,7], Stewart Fallon[8], Rainer Grün[1,8], Hannah F. James[8], Marie-Hélène Moncel[9], Ian S. Williams[8], Rachel Wood[8], Manish Arora[2]**



**Scholars endeavor to understand the relationship between human evolution and climate change. This is particularly germane for Neanderthals, who survived extreme Eurasian environmental variation and glaciations, mysteriously going extinct during a cool interglacial stage. Here, we integrate weekly records of climate, tooth growth, and metal exposure in two Neanderthals and one modern human from southeastern France. The Neanderthals inhabited cooler and more seasonal periods than the modern human, evincing childhood developmental stress during wintertime. In one instance, this stress may have included skeletal mobilization of elemental stores and weight loss; this individual was born in the spring and appears to have weaned 2.5 years later. Both Neanderthals were exposed to lead at least twice during the deep winter and/or early spring. This multidisciplinary approach elucidates direct relationships between ancient environments and hominin paleobiology.**

## INTRODUCTION

Influential studies posit a direct relationship between human evolution and ancient climate change (*1*, *2*). Recent work has linked changes in precipitation cycles in East Africa with shifts in the technological record of early *Homo sapiens*. Other scholars have noted that Neanderthals did not diversify their tool production as greatly as modern humans, despite living through several periods of extreme climate change in Eurasia (*3*, *4*). Seasonal variation is often inferred from oxygen isotopes, which vary with temperature and precipitation/evaporation cycles (*5*, *6*). Available surface water sources during prolonged periods of warm weather are enriched in naturally occurring $^{18}O$ relative to $^{16}O$, as lighter $^{16}O$ is preferentially removed during evaporation. During cool periods, evaporation is reduced, and precipitation from cold air masses contains comparatively little $^{18}O$. Thus, the standardized ratio of $^{18}O$ to $^{16}O$ ($\delta^{18}O$ value) in environmental water is higher in summer and lower in winter periods. Unfortunately, most isotopic approximations of paleoenvironments are temporally coarse relative to hominin life spans (*2*, *7*), limiting our understanding of how ancient landscape ecology directly influenced their behavior and biology.

Scholars have attempted to circumvent this limitation by quantifying oxygen isotopes in the mineral component of tooth enamel, which forms incrementally in equilibrium with seasonally varying environmental oxygen (*8*, *9*) and allows paleoclimatic inferences (*10*, *11*). Yet, concerns about the timing of elemental incorporation during tooth mineralization and the fidelity of oxygen isotopes in teeth have hindered comprehensive investigations of the fossil record (*9*, *12*, *13*). The first concern arises from the likelihood that the process of enamel mineralization, which continues after initial enamel secretion, may overprint and/or shift the elemental signature of an individual's ingestion history. This is important for studies that relate chemical records to growth increments in teeth, which form on a consistent daily basis as enamel and dentine are secreted. The second concern is whether elements in teeth that have been buried reflect the behavior of an individual during their lifetime or to what extent this biogenic signal is obscured by subsequent postmortem elemental uptake from the local environment (diagenesis).

To investigate paleoclimate and concomitant hominin biology, we use two mass spectrometry methods, addressing these methodological concerns and quantifying oxygen isotopes, trace element distributions, and tooth development in two Neanderthals and one modern human from Payre, an archeological site in the Rhone Valley (Fig. 1) (*14*, *15*). We interpret these data with the aid of a comparative sample of unburied teeth (Table 1), as well as previous results on nursing and developmental stress in living humans, captive macaques, wild orangutans, and a young Neanderthal (*16*–*18*). This approach reveals patterns of seasonal variation, Neanderthal life history, and exposure to potential environmental hazards with unprecedented detail.

## RESULTS

### Paleoclimate and mineralization offset

We find that $\delta^{18}O$ values sampled with an ion microprobe are nearly identical to those from silver phosphate microprecipitation (fig. S1), demonstrating the power of this ablative technique for recovering intratooth $\delta^{18}O$ from enamel. Oxygen isotopes in the ~250-thousand-year (ka) old Neanderthals show notable multiyear patterns reflecting winter and summer seasons (Fig. 2). The two Neanderthal teeth show clear annual $\delta^{18}O$ cycles with a maximum variation of 4.1‰ (per mil) (Payre 6) and 5.6‰ (Payre 336) over ~3 years of formation. Seasonal trends are more pronounced than in the 5.4-ka old modern human molar (Payre 1), which has higher $\delta^{18}O$ values consistent with that mid-Holocene warm period (*19*).

[1]Australian Research Centre for Human Evolution, Environmental Futures Research Institute, Griffith University, Nathan, Brisbane, Queensland 4111, Australia. [2]The Senator Frank R. Lautenberg Environmental Health Sciences Laboratory, Department of Environmental Medicine and Public Health, Icahn School of Medicine at Mount Sinai, New York, NY 10029, USA. [3]Forsyth Institute, 245 First Street, Cambridge, MA 02142, USA. [4]Department of Human Evolutionary Biology, Harvard University, Cambridge, MA 02138, USA. [5]Southern Cross GeoScience, Southern Cross University, Lismore, New South Wales 2480, Australia. [6]Department of Anthropology, New York University, New York, NY 10003, USA. [7]Department of Neuroscience, Icahn School of Medicine at Mount Sinai, New York, NY 10029, USA. [8]Research School of Earth Sciences, Australian National University, Acton, Australian Capital Territory 2601, Australia. [9]Département de Préhistoire, Institut de Paleontologie Humaine, 75013 Paris, France.
*Corresponding author. Email: tanya.smith@griffith.edu.au
†These authors contributed equally to this work.

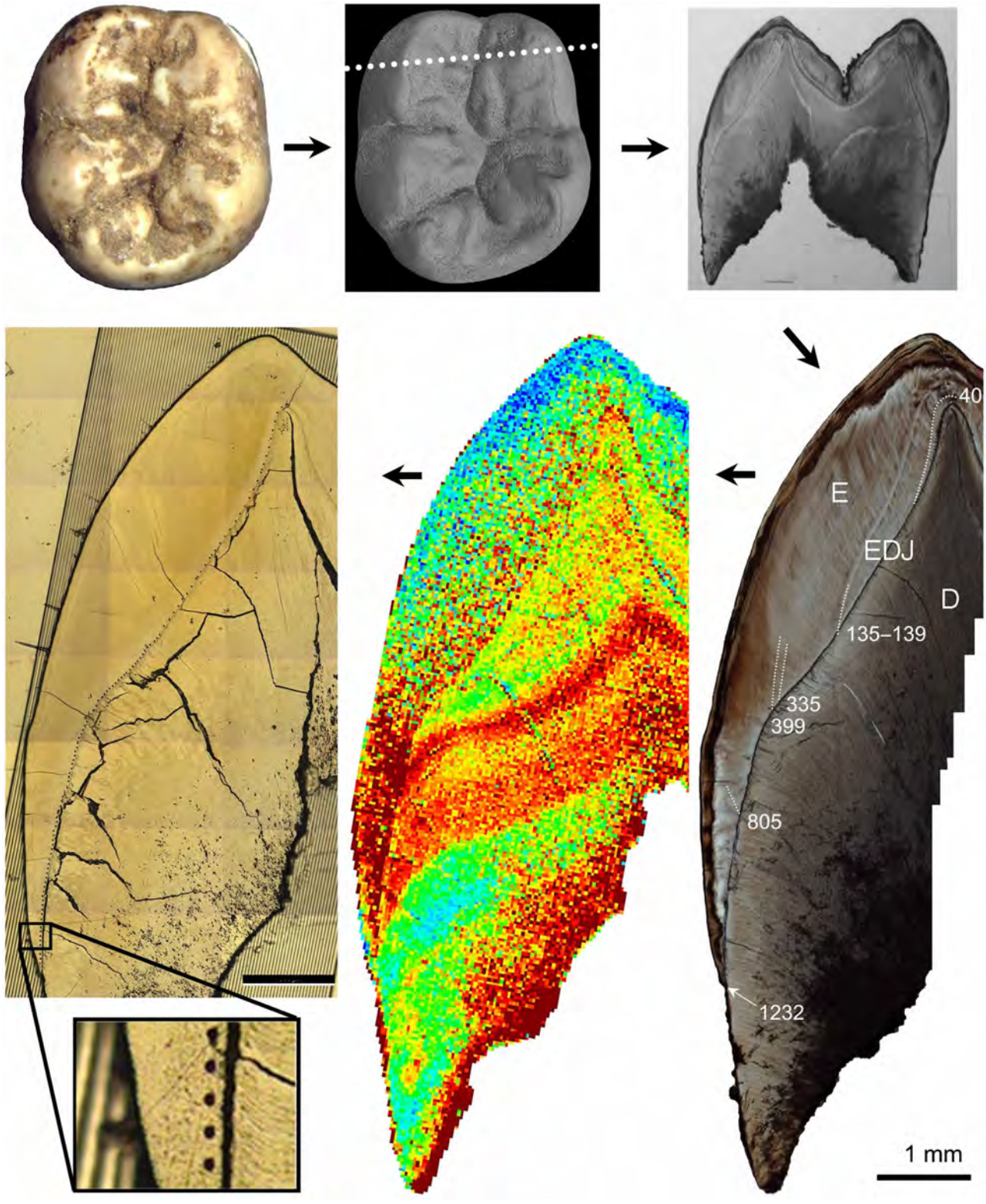


**Fig. 1. Analytical approach for Payre hominin molars in this study.** As shown clockwise from top left, this involves photography, micro–computed tomography (micro-CT) scanning and virtual sectioning, production of histological sections, identification of accentuated lines (including birth—dotted line with a postinitiation time of 40 days) and characterization of tooth formation time (in days), laser ablation elemental mapping, and secondary ion mass spectrometry (SIMS) analysis of oxygen isotopes. The inset in the lower left shows 16-μm sensitive high-resolution ion microprobe (SHRIMP) spots spaced every 50 μm immediately adjacent to the enamel-dentine junction (EDJ; dark line) and parallel 35-μm laser tracks in the embedding material around the tooth, which can be seen in the gold-coated section. The photograph and micro-CT model of Payre 1 are flipped for ease of visualization. E, enamel; D, dentine.

**Table 1. Samples and analyses reported here.** Tooth: first position, R (right) and L (left); second position, L (lower) and U (upper); third position, M (molar) and dC (deciduous canine); fourth position, 1 (first molar) and 2 (second molar). Oxygen was sampled using SHRIMP, trace elements were measured using laser ablation inductively coupled plasma mass spectrometry, and diagenesis was also assessed with laser scanning confocal fluorescence, cathodoluminescence, and Raman microspectral imaging unless noted.

| Taxon | ID | Tooth | Illustrated | Analyses subsequent to histological temporal mapping |
|---|---|---|---|---|
| *Main samples* | | | | |
| Modern human | Payre 1 | RLM1 | Figs.1 and 2 and figs. S5B and S7 | Oxygen, trace elements, and diagenesis |
| Neanderthal | Payre 6 | LLM1 | Figs. 2 and 3 and figs. S4 and S5D | Oxygen, trace elements, and diagenesis |
| Neanderthal | Payre 336 | LLM2 | Figs. 2 and 4 and figs. S5C and S6 | Oxygen, trace elements, and diagenesis |
| *Comparative samples* | | | | |
| Modern sheep | 962 | LLM2 | fig. S1 | Oxygen (SHRIMP and silver phosphate) |
| Sumatran orangutan | ZMB 83508 | RLM1 | fig. S2 | Oxygen |
| Modern sheep | CXB 11204 | LLM1 | fig. S8 | Trace elements |
| Unburied modern human | r605_1185 | RUM1 | fig. S5A | Laser scanning confocal fluorescence |
| Unburied modern human | HJM2_dC | LUdC | fig. S3 | Oxygen |

Elevated $\delta^{18}O$ values in hard tissues forming shortly after birth are likely due to enrichment from mothers' milk (*20*). The initiation of milk consumption can be identified in the Payre 1 first molar as a marked increase in $\delta^{18}O$ near the neonatal (birth) line (Fig. 2A), consistent with patterns observed in an orangutan first molar (fig. S2) and a modern human deciduous canine (fig. S3). These marked increases in oxygen are not found at the exact position of the neonatal line, which may reflect short temporal offsets due to the subsequent maturation of enamel and/or minor errors in the localization of this line. Despite the complexities of tooth mineralization, these results suggest that changes in oxygen isotope composition may be detected within a week or two of fluid ingestion.

### Biogenic signals reveal nursing history and lead exposures

Teeth have a consistent geometry of incremental growth, which can be integrated with whole-crown mapping of trace elements to elucidate primate nursing histories and illnesses (*16*–*18*). This approach is more complicated for teeth that have been buried, as diffusible elements may overprint original biogenic patterns after burial (Supplementary Text and figs. S4 to S7) (*21*, *22*). Despite this, we have detected biogenic metal incorporation that parallels tooth growth in both Neanderthals (Figs. 3 and 4). The Payre 6 first molar shows elevated barium [Ba normalized to calcium (Ba/Ca)] until 9 months of age, consistent with nursing, which then decreased for a short period, after which point enamel values were influenced by diagenesis until ~1.6 years of age (fig. S4). Subsequent barium values remained moderate until 2.5 years of age, when they fell to a minimum and remained low for the last 3 months of molar crown formation. It appears that this individual was born in the spring and weaned in the fall (Fig. 3C). There were no clear biogenic barium patterns in the Payre 336 second molar, although diagenetic barium and uranium were apparent (fig. S6). This region of France has barite ($BaSO_4$) mineral deposits near the archeological site, providing a natural source of barium that may have led to elevated values in the porous dentine and vulnerable parts of tooth crowns.

The Payre 6 Neanderthal also shows periods of lead exposure beginning after ~2.5 months of age. Slightly elevated levels persisted until a marked increase in the deep winter at 9 months of age (Fig. 3, B and C), after which values remained elevated until ~1.6 years of age (possibly related to diagenesis). At 766 days of age, lead spiked again for ~2 to 3 weeks, remaining moderately high during the last 7 months of crown formation. The second Neanderthal (Payre 336) was exposed to lead briefly during the spring, followed by an additional exposure ~108 to 176 days after completion of enamel formation, most likely during the winter or late fall (Fig. 4). The Payre 1 modern human tooth dated to 5.4 ka ago had extensive diagenetic diffusion of barium, lead, and uranium (fig. S7), prohibiting assessments of nursing or lead exposure.

### Developmental disruptions

The Payre 6 Neanderthal showed a marked developmental defect (accentuated line) in the enamel that persisted for a week (Fig. 3A), coincident with the discrete elevated barium band around 701 days of age (Fig. 3B), which occurred during the coldest part of the winter (Fig. 3C). Two marked developmental defects were evident in the Payre 336 Neanderthal's second molar, with a substantial 2-week disruption during the winter, and a week-long disruption during the subsequent fall (Fig. 4). This tooth formed between ~3 and 6 years of age (*23*), showing more developmental stress than both first molars Payre 1 and Payre 6. There were no clear disruptions to enamel formation coincident with lead bands in either Neanderthal tooth.

## DISCUSSION

### Paleoclimate and mineralization offset

Our results are consistent with archeological reconstructions of the layers that yielded the Payre Neanderthal remains (*11*, *15*). These have posited that individuals from layer F (Payre 336) and layer G

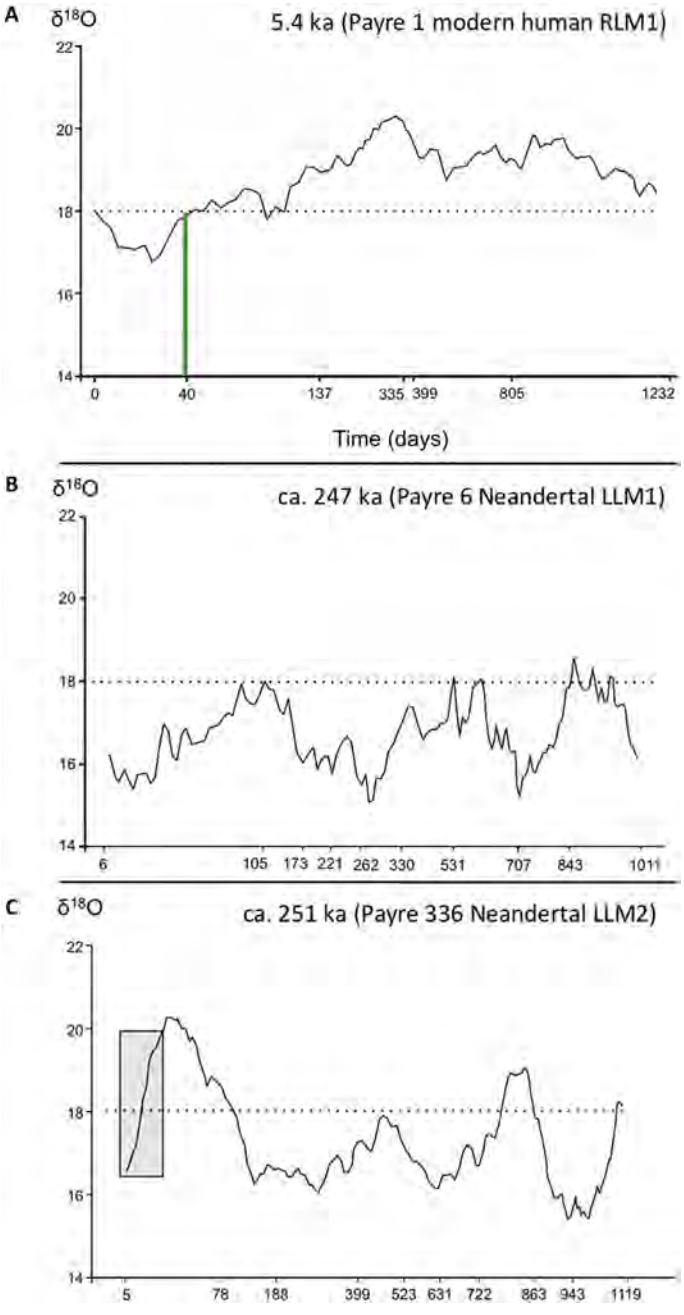


**Fig. 2. Oxygen isotopes in hominin teeth from Payre.** Oxygen isotope compositions ($\delta^{18}O$) shown on a Vienna standard mean ocean water (VSMOW) scale measured along the EDJ at a spatial scale corresponding to approximately weekly intervals. Note that the *x* axis is not linear as tooth extension begins rapidly and decreases toward the cervix. Thus, isotopic values appear stretched on the left and compressed on the right. Each plot is at the same VSMOW scale with a dotted line at 18‰ for ease of comparison across teeth. (**A**) The modern human tooth preserved a birth line (Fig. 1), indicated here as a green vertical line 40 days after tooth initiation. (**B**) The Payre 6 individual preserved a birth line (Fig. 3) formed 6 days after initiation, but it was not possible to sample prenatal enamel as this line is very close to the EDJ. (**C**) Initial $\delta^{18}O$ values (gray box) for Payre 336 might be influenced by diagenesis, as this region showed demineralization for the first 350 μm along the EDJ (fig. S5C).

(Payre 6) experienced a cold and dry climate around the start of the marine isotope stage 7 interglacial. Previous paleoenvironmental reconstructions from the Payre Neanderthal teeth report a narrower range of $\delta^{18}O$ values within and between individuals than that found in the two individuals analyzed here (*10*, *11*). Bulk enamel $\delta^{18}O$ sampling has been interpreted to demonstrate differences in habitat exploitation across archeological layers at Payre, yet this method has limited temporal resolution, yielding samples that integrate long formation times of unknown biological age. We can now constrain physical samples to regions of the tooth secreted during approximately 1 week or less over ~3 years. Our microsampling results show repeated, intra-annual seasonal $\delta^{18}O$ fluctuations of >4‰ within individuals, with marked changes occurring over time scales of months. Sequential enamel $\delta^{18}O$ measurements are more likely to capture the morphology and magnitude of environmental $\delta^{18}O$ variation in temperate environments where seasonal $\delta^{18}O$ fluctuations are large and dominated by relatively simple winter-summer regimes (*9*).

The integration of developmental mapping and fine-scaled whole-crown elemental quantification provides a powerful approach to clarifying the timing of elemental incorporation and diagenetic elemental intrusion, two concerns that have limited previous investigations of hominin fossils. Substantial changes in $\delta^{18}O$ values appear in the enamel within a few days to weeks of the onset of nursing. Complementary experimental evidence is apparent in fig. S1, as water $\delta^{18}O$ values were artificially lowered at 202 days of age and increased at 262 days of age, which are reflected in marked changes in enamel $\delta^{18}O$ within a few days of these changes. We find a comparable phenomenon with barium patterns, as elevated values due to initial nursing begin to appear in the enamel no more than a few weeks before birth (fig. S8), as has been previously shown in other primate samples forming during the birth process (*16*, *18*). This offset between prenatal enamel and the neonatal line is due to overprinting of the prenatal region by subsequent postnatal mineral incorporation, creating a minor elemental shift relative to the timing of growth line formation during secretion. Lastly, lead exposures in the enamel and dentine of both Neanderthals also manifest nearly synchronously (Figs. 3 and 4). Thus, mineralization of the innermost enamel does not appear to substantially mask or shift biogenic oxygen isotope ratios or certain trace element inputs. Reconstructions of seasonality, nursing behavior, and lead exposure can be directly related to tooth formation timing.

## Neanderthal nursing history, lead exposure, and health

These results also provide novel insight into the reproductive biology of Neanderthals, including the seasons of birth and weaning, as well as the duration of nursing—a key determinant of population growth and life history. It appears that the Payre 6 individual was born in the spring and weaned in the fall. Mammals, including humans, show seasonal birth patterns that relate to environmental cycles (*24*, *25*). Our results for Payre 6 are consistent with the broad mammalian pattern of bearing offspring during periods of increased food availability. Sustained low barium values in the final 3 months of tooth formation indicate that this Neanderthal ceased nursing when it was 2.5 years old, which is similar to the average age of weaning in nonindustrial human populations (*26*). Our previous research on a ~100-ka-old Belgian Neanderthal identified an abrupt cessation of nursing at 1.2 years of age (*16*). It is likely that the result from Payre 6 provides a more normative weaning age for a Neanderthal, as the

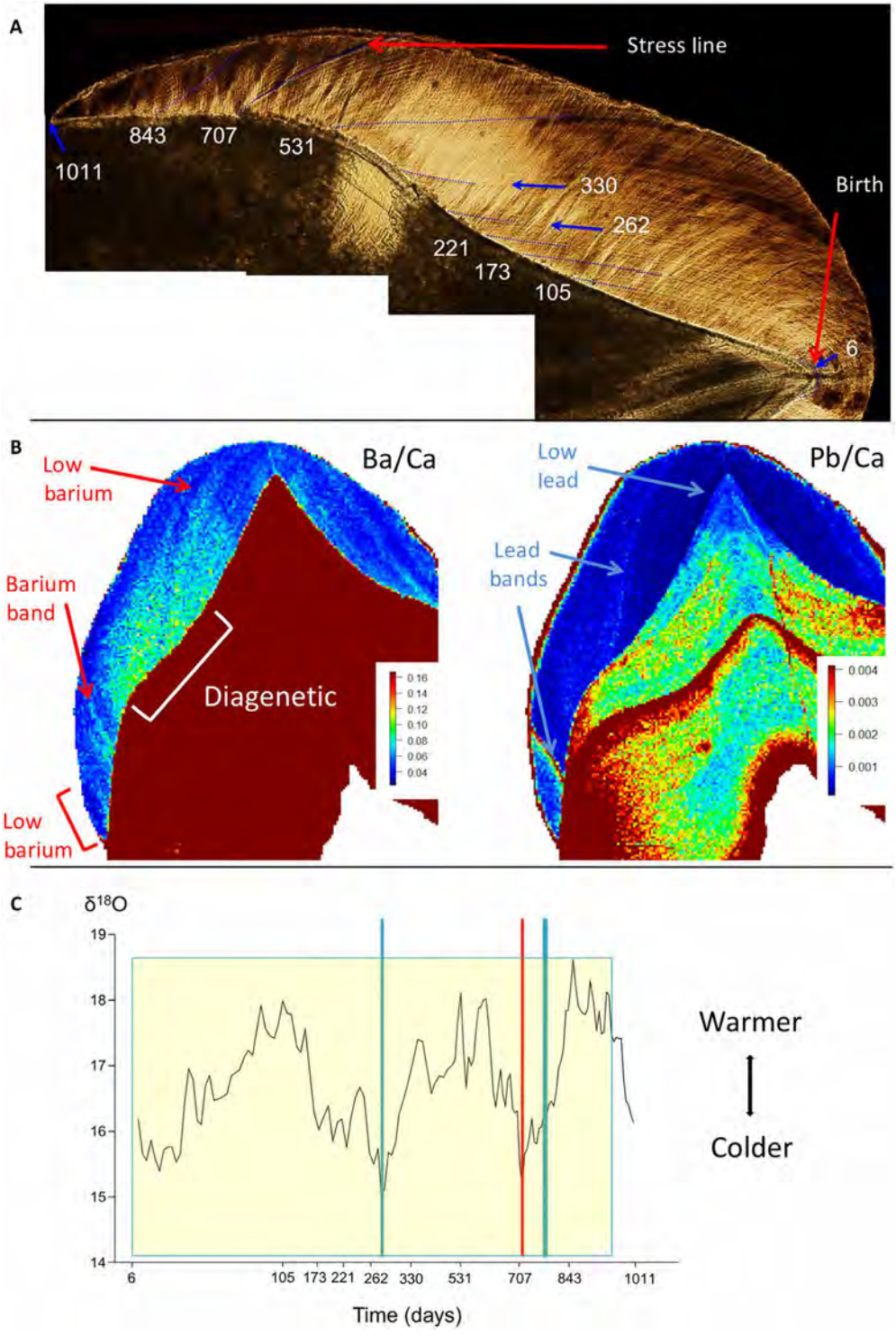


**Fig. 3. Integration of developmental, elemental, and isotopic data for Payre 6.** (**A**) First molar distobuccal cusp enamel development (time in days), including the birth line 6 days after enamel initiation and a marked week-long stress at 707 days (701 days of age). (**B**) Calcium-normalized barium (Ba/Ca) and lead (Pb/Ca) maps, with biogenic patterns indicated by arrows and brackets. The Ba/Ca map on the left shows an artificially elevated region (fig. S4), a biogenic band at 707 days after initiation, and sustained minimum values in the cervical region most likely due to weaning at 2.5 years of age. On the right, the first elevated Pb band at ~286 days after initiation corresponds to the beginning of the low Ba region in the cuspal enamel, while the second band was formed at ~772 days. It was not possible to sample the prenatal enamel exclusively as the birth line is too close to the EDJ (~20 μm away at maximum distance); thus, each innermost 35-μm laser spot includes both pre- and postnatal enamel above the dentine horn. (**C**) Oxygen isotope values over 2.8 years. The yellow box indicates elevated Ba/Ca values that cease 3 months before molar cusp completion. The blue vertical lines indicate the formation of the lead bands, while the red line corresponds to the elevated barium band. The other distal cusp of this tooth completed formation a few months earlier and thus does not provide a postweaning signal.

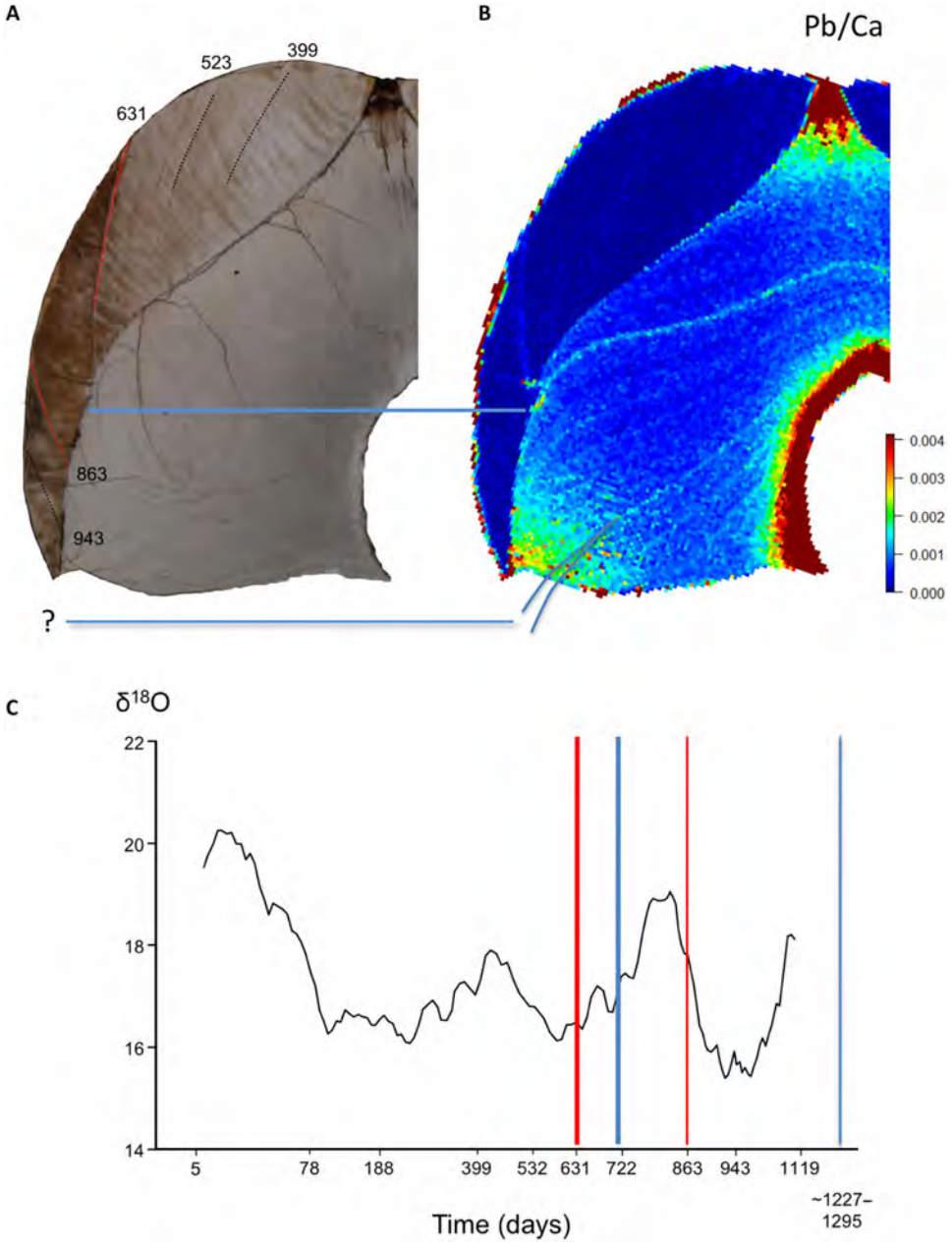


**Fig. 4. Integration of developmental, elemental, and isotopic data for Payre 336.** (**A**) Second molar mesiobuccal cusp development (time in days), including a marked ~2-week developmental defect at 631 days and a week-long defect at 863 days (red dotted lines). (**B**) Calcium-normalized lead (Pb/Ca) map, with biogenic patterns indicated by blue lines registered to the temporal map. The first biogenic lead band formed at ~722 days after tooth initiation, while the second band formed after cusp completion (>1119 days). Projections of the curvature of growth lines suggest that it would have formed ~108 to 176 days after completion. (**C**) Oxygen isotope values ($\delta^{18}O$) over 3 years of tooth formation. Vertical lines on the isotopic plot reveal timing of developmental defects (red lines) and biogenic lead exposures (blue lines). No biogenic barium information was available for this tooth.

Belgian individual did not show the progressive decline in barium seen when humans, apes, and monkeys gradually transition from mothers' milk to solid foods. Instead, there was a marked disruption of enamel formation at 1.2 years of age and an immediate steep decrease of barium at this point—a pattern also seen in a captive macaque that was prematurely separated from its mother before natural weaning. Additional studies are needed to establish a mean age for Neanderthal weaning, as well as whether this differs from contemporaneous modern humans or varies across the diverse Eurasian environments Neanderthals inhabited.

Repeated lead exposures during childhood in the two Neanderthals are the earliest such evidence in hominin remains. The intensity of lead signals in prominent bands exceeds levels elsewhere in the teeth by a factor of 10. These high and acute lead lines are indicative of short-term exposure from ingestion of contaminated food or water or inhalation from fires containing lead (*27*). Lead can also

come from mothers' milk (*28*), but the divergent patterns of barium and lead in Payre 6 and the acute lead bands in both individuals suggest that mothers' milk was not the primary source of exposure. It is plausible that the lead in Payre 6 came from nonmilk liquids beginning at ~2.5 months of age, increasing with solid food consumption in the winter from 9 months of age and, again, in the late winter/early spring of the following year. At least two lead mines are located within 25 km of the site (*29*), consistent with estimates of routine foraging distances (*11*). Periods of lead exposure during the childhoods of these two French Neanderthals are remarkable, as biogenic lead bands were not apparent in the ~100-ka-old Belgian individual discussed above, and decades of research have shown that there is no safe level for lead in humans and other animals.

Lead exposures did not result in the formation of obvious developmental defects in the Payre Neanderthals' enamel. We found a marked defect in Payre 6 coincident with a short-term barium elevation at approximately 701 days of age (Fig. 3, A and B). It appears that during the coldest time of winter, this young individual experienced heightened skeletal remineralization. Trace elements can be released into the bloodstream from skeletal stores, exemplified by the phenomenon of lead mobilization in parallel with calcium during human lactation (*28*). The pattern of acute barium elevation coincident with a developmental defect in Payre 6 is akin to that seen in captive rhesus macaques after they had ceased nursing (*17*). Several of these macaques lost weight during severe illnesses, mobilizing trace elements that had been stored in their bones, which were recorded in concurrently forming tooth enamel and dentine. While the Payre 6 individual appeared to have continued nursing throughout the disruption at ~701 days of age, the short spike in barium concentration and the presence of a strong enamel disruption are more consistent with acute illness and associated weight loss than a transient increase in maternal milk consumption.

The approach detailed here allows more robust explorations of Neanderthal paleobiology and prehistoric environmental conditions than conventional assessment of associated fauna or geological signatures (*30*). Broader applications may also help to clarify the purported relationship between climate variation and technological innovation in members of the genus *Homo* (*1*, *2*). Although it is unclear whether and how cold stress or neurotoxicant exposure routinely affected the health of Neanderthals, scholars have noted the frequent occurrence of developmental defects in their teeth (*23*, *31*). Several common explanations for these defects, including weaning stress and illness, can now be probed through developmentally informed barium mapping. While diagenetic modification may prohibit characterizations of teeth interred near naturally occurring barium sources, the quantification of diagenetically resistant oxygen isotopes provides complementary insights into the lives of young hominins.

## MATERIALS AND METHODS

### Payre samples

We used three teeth from the site of Payre in southeastern France originally believed to derive from level D (Payre 1), level F (Payre 336), and level G (Payre 6) (*14*). During the course of this study, it became apparent that Payre 1 (Fig. 1), initially identified as a Neanderthal, was an intrusive modern human right lower first molar from a recent occupation of the site. To determine its age, an embedded half of the tooth was subjected to radiocarbon dating at the Australian National University, as detailed in the following section. Thermoluminescence dating applied to numerous fragments of in situ burnt flints associated with Neanderthal dental remains from level F and level G yielded ages of 251 ± 25 and 247 ± 29 ka old, respectively (*15*).

### Radiocarbon dating of Payre 1

The embedding media and root surface were first removed with a drill, and the coronal dentine was sampled from within the tooth cap. Collagen was extracted and purified from the dentine following an ultrafiltration protocol. Dentine powder was demineralized in 0.5 M HCl overnight and then washed in 0.1 M NaOH for 30 min and 0.5 M HCl for 1 hour, rinsing with ultrapure water between treatments. Samples were then gelatinized in 0.001 M HCl at 70°C for 20 hours, filtered using an Ezee-Filter to remove insoluble contaminants, and then ultrafiltered with a cleaned Vivaspin VS15turbo 30,000 molecular weight cutoff ultrafilter to remove small contaminants. For dating, the freeze-dried collagen was combusted in a sealed quartz tube with CuO wire and Ag foil. The $CO_2$ generated was then cryogenically purified and collected for graphitization with $H_2$ over an Fe catalyst and analyzed on a National Electrostatics Corporation single-stage accelerator mass spectrometer (*32*). Dates were calculated according to (*33*), and a collagen-specific background correction was made. Dates have been calibrated against IntCal13 (*34*) in OxCal (*35*). The 95.4% probability range is 5355 to 5453 years. To assess the collagen quality, carbon and nitrogen elemental and stable isotope abundances were obtained from a second aliquot of collagen using an ANCA GSL elemental analyzer connected to a Sercon 20-22 isotope ratio mass spectrometer (IRMS) operating in continuous flow mode, using an in-house gelatin reference and corrected against USGS40 and USGS41. Collagen quality was good, with ~5 mg and 3 weight % collagen recovered from the dentine sample. %C and C/N ratio are representative of bone collagen (*36*).

### Tooth positions of Payre 6 and Payre 336

We reassessed the morphology of the two Neanderthal teeth, which were originally reported to be a lower right second molar (Payre 6) and a worn first or second left lower molar (Payre 336) (*14*). Both teeth have mesial and distal wear facets, suggesting that they are unlikely to be third molars. Quantification of the relative cusp areas of these teeth indicates that Payre 6 shows a configuration most similar to Neanderthal lower first molars, while Payre 336 aligns with Neanderthal lower second molars (table S1) (*37*). The attribution of Payre 6 as a lower left first molar is further supported by the similarity between this tooth and several early Neanderthal lower first molars from Sima de los Huesos [e.g., (*38*), p. 44]. The attribution of Payre 336 as a lower left second molar is further supported by the similarity in size with lower second molars from Sima de los Huesos (table S2) (*39*). This is consistent with morphological characteristics including the crown outline, which is less oval than most Neanderthal first molars but more like second molars, as well as the distal position from which the hypoconulid fissures originate and its centrally placed position along the distal margin.

### Tooth development and trace element analyses

The three hominin teeth (Payre 1, Payre 6, and Payre 336) were first subjected to micro-CT scanning with a Skycan 1272 to guide the production of histological sections, as detailed in (*40*) (Fig. 1). Accentuated line ages were spatiotemporally mapped from incremental features in the enamel formed after the neonatal (birth) line of first molars Payre 1 and Payre 6 (Figs. 1 and 3) [following (*16*–*18*)]. Developmental

time was also assessed from two histological sections of Payre 336, a moderately worn second molar tooth (Fig. 4). Local extension rates were calculated as the distance along the EDJ divided by the duration of tooth formation to assess the timing of changes in trace element distributions that occurred between accentuated lines. Elemental analysis follows previously published methods (*16*, *18*). Data points for calcium-normalized Ba, Pb, and U correspond to a pixel size of approximately 35 μm by 35 μm, save for fig. S8, which reflects a pixel size of 15 μm by 15 μm.

### Isotopic analysis

Oxygen isotopic compositions were measured using the SHRIMP SI at the Australian National University, which is specially configured for the stable isotope analysis of geological materials (*41*, *42*). Polished histological sections of the three Payre hominins and several modern samples were cleaned with petroleum benzene, warm RBS detergent solution, and ultrapure $H_2O$; dried for ≥24 hours in a 60°C vacuum oven; and coated with a thin (~10 nm) layer of high-purity Al (and/or Au) before they were placed in the SHRIMP SI under high vacuum for ~12 hours prior to SIMS analysis. A ~3-nA, 15-kV beam of positive Cs ions was used to sequentially sputter a series of 16-μm-diameter spots in the innermost enamel adjacent to the EDJ from the dentine horn to the cervix. Negative O secondary ions were extracted at 10 kV, mass separated at ~3000R, and measured in current mode using a multiple collector equipped with dual Faraday cups [resistors, $10^{11}$ ohms ($^{16}O$) and $10^{12}$ ohms ($^{18}O$)]. Charge on the sample surface was neutralized using a 1.2-kV focused electron beam. Each analysis consisted of 2 min of preconditioning, during which electrometer baselines were measured, followed by optimization of the beam steering and 6 × 20-s measurements of $^{18}O/^{16}O$, giving a precision of ~0.1‰ ($^{16}O$, ~1.9 GHz). Electron-induced secondary ion emission was measured before and after each analysis. $\delta^{18}O$ values were calculated relative to mineral apatite standard Durango3 [9.8‰$_{VSMOW}$; (*43*)] that was measured repeatedly over the course of the approximately 14- to 23-hour period of data collection for each tooth (SD, ~0.2‰).

Spots were spaced 50 μm apart for the first 4 to 5 mm of Payre 6 and Payre 336, decreasing to 30 μm in the cervical region. Postnatal extension rates (EDJ length divided by formation time) in the first 4 mm of the Neanderthal teeth ranged from 20 to 7 μm/day, decreasing to 6 μm/day; thus, each spot reflects ~1 to 2.5 days of secretion with an interval of ~2 to 8 days between spots. For Payre 1, spots were spaced 100 μm apart for the first 3 mm, decreasing to 50-μm spacing in the middle and cervical enamel. Extension rates for the first 3 mm of Payre 1 ranged from 31 to 29 μm/day, dropping to 13 to 7 μm/day in the middle and cervical enamel, respectively. Here, each spot reflects ~0.5 to 2 days of secretion with an interval of ~3 to 7 days between spots.

A comparison was made between SIMS and silver phosphate oxygen recovery in parallel sections of a sheep second molar tooth aligned via a notch on the tooth (fig. S1). The sheep was raised under controlled conditions in Bedford, MA, and calcein labeling provided temporal control for $\delta^{18}O$ analyses at discrete locations within the enamel crown (*9*, *13*). The SHRIMP SI spot size was 30 μm, and measurements were spaced 500 μm apart for the first 33.5 mm of the tooth crown, with twofold sampling at 16.5 and 21.5 mm from the enamel cusp tip. SIMS measurements do not extend to the end of the cervical margin of the enamel. Phosphate $\delta^{18}O$ measurements were made from 1.5 mm by 0.3 mm by 0.6 mm blocks of the inner enamel above the EDJ diced from the cusp to the cervix. Measurements were conducted using silver phosphate microprecipitation and thermal conversion elemental analyzer-IRMS at the University of Chicago.

## SUPPLEMENTARY MATERIALS

Supplementary material for this article is available at http://advances.sciencemag.org/cgi/content/full/4/10/eaau9483/DC1

Supplementary Text

Fig. S1. Validation of SHRIMP sampling of oxygen isotopes ($\delta^{18}O$) from the phosphate component of tooth enamel.

Fig. S2. Oxygen isotopes ($\delta^{18}O$) in the first molar of a wild Sumatran orangutan.

Fig. S3. Oxygen isotopes ($\delta^{18}O$) in a modern human deciduous canine.

Fig. S4. Comparison of calcium-normalized distributions of barium and uranium in the Neanderthal first molar (Payre 6).

Fig. S5. Confocal fluorescence images revealing extensive autofluorescence in enamel (red arrows).

Fig. S6. Comparison of calcium-normalized distributions of barium and uranium in the Neanderthal second molar (Payer 336).

Fig. S7. Comparison of calcium-normalized distributions of barium, uranium, and lead in the 5.4-ka-old modern human tooth (Payre 1).

Fig. S8. Illustration of limited overprinting of calcium-normalized barium during enamel maturation in a sheep that died at 21 days of age.

Table S1. Relative cusp areas of Payre 6, Payre 336, and a comparative Neanderthal sample (*37*).

Table S2. Crown size (in millimeters) of Payre 6, Payre 336, and a comparative sample of classic Neanderthals (Neanderthal columns) and early Neanderthals from Sima de los Huesos (SH columns) (*37*–*39*, *58*).

References (*44*–*58*)

## REFERENCES AND NOTES


1. R. Potts, Evolution and climate variability. *Science* **273**, 922–923 (1996).
2. R. Potts, A. K. Behrensmeyer, J. T. Faith, C. A. Tryon, A. S. Brooks, J. E. Yellen, A. L. Deino, R. Kinyanjui, J. B. Clark, C. M. Haradon, N. E. Levin, H. J. M. Meijer, E. G. Veatch, R. B. Owen, R. W. Renaut, Environmental dynamics during the onset of the Middle Stone Age in eastern Africa. *Science* **360**, 86–90 (2018).
3. J.-P. Bocquet-Appel, A. Tuffreau, Technological responses of Neanderthals to macroclimatic variations (240,000–40,000 BP). *Hum. Biol.* **81**, 287–307 (2009).
4. S. E. Churchill, *Thin on the Ground: Neandertal Biology, Archeology, and Ecology* (Wiley, 2014).
5. W. Dansgaard, Stable isotopes in precipitation. *Tellus* **16**, 436–468 (1964).
6. G. J. Bowen, Isoscapes: Spatial pattern in isotopic biogeochemistry. *Annu. Rev. Earth Planet. Sci.* **38**, 161–187 (2010).
7. B. H. Passey, N. E. Levin, T. E. Cerling, F. H. Brown, J. M. Eiler, High-temperature environments of human evolution in East Africa based on bond ordering in paleosol carbonates. *Proc. Natl. Acad. Sci. U.S.A.* **107**, 11245–11249 (2010).
8. S. A. Blumenthal, T. E. Cerling, K. L. Chritz, T. G. Bromage, R. Kozdon, J. W. Valley, Stable isotope time-series in mammalian teeth: In situ $\delta^{18}O$ from the innermost enamel layer. *Geochim. Cosmochim. Acta* **124**, 223–236 (2014).
9. D. R. Green, T. M. Smith, G. M. Green, F. B. Bidlack, P. Tafforeau, A. S. Colman, Quantitative reconstruction of seasonality from stable isotopes in teeth. *Geochim. Cosmochim. Acta* **235**, 483–504 (2018).
10. M. Aubert, I. S. Williams, K. Boljkovac, I. Moffat, M.-H. Moncel, E. Dufour, R. Grün, In situ oxygen isotope micro-analysis of faunal material and human teeth using a SHRIMP II: A new tool for palaeo-ecology and archaeology. *J. Archaeol. Sci.* **39**, 3184–3194 (2012).
11. H. Bocherens, M. D.-Z. Bonilla, C. Daujeard, P. Fernandes, J.-P. Raynal, M.-H. Moncel, Direct isotopic evidence for subsistence variability in Middle Pleistocene Neanderthals (Payre, southeastern France). *Quat. Sci. Rev.* **154**, 226–236 (2016).
12. T. M. Smith, P. Tafforeau, New visions of dental tissue research: Tooth development, chemistry, and structure. *Evol. Anthropol.* **17**, 213–226 (2008).
13. D. R. Green, G. M. Green, A. S. Colman, F. B. Bidlack, P. Tafforeau, T. M. Smith, Synchrotron imaging and Markov chain Monte Carlo reveal tooth mineralization patterns. *PLOS ONE* **12**, e0186391 (2017).
14. M.-H. Moncel, S. Condemi, The human remains of the site of Payre (S-E France, MIS 7-5). Remarks on stratigraphic position and interest. *Anthropologie* **45**, 19–30 (2007).
15. H. Valladas, N. Mercier, L. K. Ayliffe, C. Falguères, J.-J. Bahain, J.-M. Dolo, L. Froget, J.-L. Joron, H. Masaoudi, J.-L. Reyss, M.-H. Moncel, Radiometric dates for the Middle Palaeolithic sequence of Payre (Ardèche, France). *Quat. Geochronol.* **3**, 377–389 (2008).
16. C. Austin, T. M. Smith, A. Bradman, K. Hinde, R. Joannes-Boyau, D. Bishop, D. J. Hare, P. Doble, B. Eskenazi, M. Arora, Barium distributions in teeth reveal early-life dietary transitions in primates. *Nature* **498**, 216–219 (2013).
17. C. Austin, T. M. Smith, R. M. Z. Farahani, K. Hinde, E. A. Carter, J. Lee, P. A. Lay, B. J. Kennedy, B. Sarrafpour, R. J. Wright, R. O. Wright, M. Arora, Uncovering system-specific stress signatures in primate teeth with multimodal imaging. *Sci. Rep.* **6**, 18802 (2016).

18. T. M. Smith, C. Austin, K. Hinde, E. V. Vogel, M. Arora, Cyclical nursing patterns in wild orangutans. *Sci. Adv.* **3**, e1601517 (2017).
19. F. McDermott, S. Frisia, Y. Huang, A. Longinelli, B. Spiro, T. H. E. Heaton, C. J. Hawkesworth, A. Borsato, E. Keppens, I. J. Fairchild, K. van der Borg, S. Verheyden, E. Selmo, Holocene climate variability in Europe: Evidence from $\delta^{18}O$, textural and extension-rate variations in three speleothems. *Quat. Sci. Rev.* **18**, 1021–1038 (1999).
20. T. Tsutaya, M. Yoneda, Reconstruction of breastfeeding and weaning practices using stable isotope and trace element analyses: A review. *Am. J. Phys. Anthropol.* **156**, 2–21 (2015).
21. B. Reynard, V. Balter, Trace elements and their isotopes in bones and teeth: Diet, environments, diagenesis, and dating of archeological and paleontological samples. *Palaeogeogr. Palaeoclimatol. Palaeoecol.* **416** 4–16 (2014).
22. J. V. Dudgeon, M. Tromp, B. K. Hanks, A. V. Epimakhov, Investigating biogenic versus diagenetic trace element incorporation in archaeological mineralized tissues in LA-ICP-MS, in *Recent Advances in Laser Ablation ICP-MS for Archaeology*, L. Dussubieux, M. Golitko, B. Gratuze, Eds. (Springer, 2016), pp. 323–341.
23. T. M. Smith, P. Tafforeau, D. J. Reid, J. Pouech, V. Lazzari, J. P. Zermeno, D. Guatelli-Steinberg, A. J. Olejniczak, A. Hoffman, J. Radovčić, M. Makaremi, M. Toussaint, C. Stringer, J.-J. Hublin, Dental evidence for ontogenetic differences between modern humans and Neanderthals. *Proc. Natl. Acad. Sci. U.S.A.* **107**, 20923–20928 (2010).
24. F. H. Bronson, Seasonal variation in human reproduction: Environmental factors. *Q. Rev. Biol.* **70**,141–164 (1995).
25. M. Martinez-Bakker, K. M. Bakker, A. A. King, P. Rohani, Human birth seasonality: Latitudinal gradient and interplay with childhood disease dynamics. *Proc. Biol. Sci.* **281**, 20132438 (2014).
26. D. W. Sellen, D. B. Smay, Relationship between subsistence and age at weaning in "preindustrial" societies. *Hum. Nat.* **12**, 47–87 (2001).
27. L. J. Kristensen, M. P. Taylor, Fields and forests in flames: Lead and mercury emissions from wildfire pyrogenic activity. *Environ. Health Perspect.* **120**, a56–a57 (2012).
28. B. L. Gulson. K. R. Mahaffey, C. W. Jameson, K. J. Mizon, M. J. Korsch, M. A. Cameron, J. A. Eisman, Mobilization of lead from the skeleton during the postnatal period is larger than during pregnancy. *J. Lab. Clin. Med.* **131**, 324–329 (1998).
29. M. Auragues, in *Etude Géologique de la Bordure Nord-Ardéchoise du Massif Central* (Bureau de Recherche Géologiques et Minières, 1961), pp. 75-82.
30. E. Discamps, A. Royer, Reconstructing palaeoenvironmental conditions faced by Mousterian hunters during MIS 5 to 3 in southwestern France: A multi-scale approach using data from large and small mammal communities. *Quat. Int.* **433**, 64–87 (2017).
31. D. Guatelli-Steinberg, A. Stinespring-Harris, D. J. Reid, C. S. Larsen, D. L. Hutchinson, T. M. Smith, Chronology of linear enamel hypoplasia formation in the Krapina Neanderthals. *Paleo Anthropol.* **2014**, 431–445 (**2014**).
32. S. J. Fallon, L. K. Fifield, J. M. Chappell, The next chapter in radiocarbon dating at the Australian National University: Status report on the single stage AMS. *Nucl. Instrum. Methods Phys. Res. B* **268**, 898–901 (2010).
33. M. Stuiver, H. A. Polach, Reporting of $^{14}C$ data. *Radiocarbon* **19**, 355–363 (1977).
34. P. J. Reimer, E. Bard, A. Bayliss, J. W. Beck, P. G. Blackwell, C. B. Ramsey, C. E. Buck, H. Cheng, R. L. Edwards, M. Friedrich, P. M. Grootes, T. P. Guilderson, H. Haflidason, I. Hajdas, C. Hatté, T. J. Heaton, D. L. Hoffmann, A. G. Hogg, K. A. Hughen, K. F. Kaiser, B. Kromer, S. W. Manning, M. Niu, R. W. Reimer, D. A. Richards, E. M. Scott, J. R. Southon, R. A. Staff, C. S. M. Turney, J. van der Plich, IntCal13 and Marine13 radiocarbon age calibration curves 0-50,000 years cal BP. *Radiocarbon* **55**, 1869–1887 (2013).
35. C. B. Ramsey, Bayesian analysis of radiocarbon dates. *Radiocarbon* **51**, 337–360 (2009).
36. G. J. Van Klinken, Bone collagen quality indicators for palaeodietary and radiocarbon measurements. *J. Archaeol. Sci.* **26**, 687–695 (1999).
37. S. Bailey, "*Neandertal Dental Morphology: Implications for Modern Human Origins*," thesis, Arizona State University (2002).
38. M. Martinón-Torres, J. M. Bermúdez de Castro, A. Gómez-Robles, L. Prado-Simón, J. L. Arsuaga, Morphological description and comparison of the dental remains from Atapuerca-Sima de los Huesos site (Spain). *J. Hum. Evol.* **62**, 7–58 (2012).
39. J. M. Bermúdez de Castro, The Atapuerca dental remains. New evidence (1987-1991 excavations) and interpretations. *J. Hum. Evol.* **24**, 339–371 (1993).
40. T. M. Smith, M. Toussaint, D. J. Reid, A. J. Olejniczak, J.-J. Hublin, Rapid dental development in a Middle Paleolithic Belgian Neanderthal. *Proc. Natl. Acad. Sci. U.S.A.* **104**, 20220–20225 (2007).
41. T. R. Ireland, S. W. J. Clement, W. Compston, J. J. Foster, P. Holden, B. Jenkins, P. Lanc, N. Schram, I. S. Williams, Development of SHRIMP. *Aust. J. Earth Sci.* **55**, 937–954 (2008).
42. R. B. Ickert, J. Hiess, I. S. Williams, P. Holden, T. R. Ireland, P. Lanc, N. Schram, J. J. Foster, S. W. Clement, Determining high precision, in-situ, oxygen isotope ratios with a *SHRIMP II*: Analyses of MPI-DING silicate-glass reference materials and zircon from contrasting granites. *Chem. Geol.* **257**, 114–128 (2008).
43. J. A. Trotter, I. S. Williams, A. Nicora, M. Mazza, M. Rigo, Long-term cycles of Triassic climate change: A new $\delta^{18}O$ record from conodont apatite. *Earth Planet. Sci. Lett.* **415**, 165–174 (2015).
44. R. Grün, M. Aubert, R. Joannes-Boyau, M.-H. Moncel, High resolution analysis of uranium and thorium concentration as well as U-series isotope distributions in a Neanderthal tooth from Payre (Ardeche, France) using laser ablation ICP-MS. *Geochim. Cosmochim. Acta* **72**, 5278–5290 (2008).
45. P. Tafforeau, I. Bentaleb, J.-J. Jaeger, C. Martin, Nature of laminations and mineralization in rhinoceros enamel using histology and X-ray synchrotron microtomography: Potential implications for palaeoenvironmental isotopic studies. *Palaeogeogr. Palaeoclimatol. Palaeoecol.* **246**, 206–227 (2007).
46. M. J. Kohn, T. E. Cerling, Stable isotope compositions of biological apatite, in *Phosphates: Geochemical, Geobiological, and Materials Importance*, M. J. Kohn, J. Rakovan, J. M. Hughes, Eds. (Mineralogical Society of America, 2002), vol. 48, pp. 455–488.
47. Z. D. Sharp, T. E. Cerling, A laser GC-IRMS technique for in situ stable isotope analyses of carbonates and phosphates. *Geochim. Cosmochim. Acta* **60**, 2909–2916 (1996).
48. E. Pucéat, M. M. Joachimski, A. Bouilloux, F. Monna, A. Bonin, S. Motreuil, P. Morinière, S. Hénard, J. Mourin, G. Dera, D. Quesne, Revised phosphate–water fractionation equation reassessing paleotemperatures derived from biogenic apatite. *Earth Planet. Sci. Lett.* **298**, 135–142 (2010).
49. C. Lécuyer, R. Amiot, A. Touzeau, J. Trotter, Calibration of the phosphate $\delta^{18}O$ thermometer with carbonate–water oxygen isotope fractionation equations. *Chem. Geol.* **347**, 217–226 (2013).
50. S. J. Chang, R. E. Blake, Precise calibration of equilibrium oxygen isotope fractionations between dissolved phosphate and water from 3 to 37 °C. *Geochim. Cosmochim. Acta* **150**, 314–329 (2015).
51. M. Pellegrini, J. A. Lee-Thorp, R. E. Donahue, Exploring the variation of the $\delta^{18}O_p$ and $\delta^{18}O_c$ relationship in enamel increments. *Palaeogeogr. Palaeoclimatol. Palaeoecol.* **310**, 71–83 (2011).
52. R. B. Trayler, M. J. Kohn, Tooth enamel maturation reequilibrates oxygen isotope compositions and supports simple sampling methods. *Geochim. Cosmochim. Acta* **198**, 32–47 (2017).
53. Y. Wang, T. E. Cerling, A model of fossil tooth and bone diagenesis: Implications for paleodiet reconstruction from stable isotopes. *Palaeogeogr. Palaeoclimatol. Palaeoecol.* **107**, 281–289 (1994).
54. A. Zazzo, C. Lécuyer, A. Mariotti, Experimentally-controlled carbon and oxygen isotope exchange between bioapatites and water under inorganic and microbially-mediated conditions. *Geochim. Cosmochim. Acta* **68**, 1–12 (2004).
55. R. L. Quinn, Influence of Plio-Pleistocene basin hydrology on the Turkana hominin enamel carbonate $\delta^{18}O$ values. *J. Hum. Evol.* **86**, 13–31 (2015).
56. E. Krzemińska, A. Sołtysiak, Z. J. Czupyt, Reconstructing seasonality using $\delta^{18}O$ in incremental layers of human enamel: A test of the analytical protocol developed for SHRIMP IIe/MC ion microprobe. *Geol. Q.* **61**, 370–383 (2017).
57. T. M. Smith, Dental development in living and fossil orangutans. *J. Hum. Evol.* **94**, 92–105 (2016).
58. M. Meyer, J.-L. Arsuaga, C. de Filippo, S. Nagel, A. Aximu-Petri, B. Nickel, I. Martínez, A. Gracia, J. M. Bermúdez de Castro, E. Carbonell, B. Viola, J. Kelso, K. Prüfer, S. Pääbo, Nuclear DNA sequences from the Middle Pleistocene Sima de los Huesos hominins. *Nature* **531**, 504–507 (2016).


**Acknowledgments:** M. Aubert, L. Cook, J. Huntley, J. Kingston, J. Trotter, and M. Willems provided helpful comments on this research. T. Ireland provided logistical support at the Australian National University. Technical assistance was provided by K. Sokolowski and B. Tse at the Preclinical Imaging Core Facility at the Translational Research Institute, funding support for which came from Therapeutic Innovation Australia, under the National Collaborative Research Infrastructure Strategy. We also acknowledge the assistance of M. Aldenderfer and several anonymous reviewers. **Funding:** This work was funded by Griffith University, the Australian National University, and the Icahn School of Medicine at Mount Sinai. **Author contributions:** T.M.S., C.A., D.R.G., R.J.-B., R.G., M.-H.M., I.S.W., and M.A. designed this study. T.M.S., C.A., D.R.G., R.J.-B., S.B., D.D., S.F., R.G., H.F.J., I.S.W., R.W., and M.A. collected and analyzed data. T.M.S. and D.R.G. wrote the paper with contributions from C.A., R.J.-B., S.B., S.F., H.F.J., I.S.W., R.W., and M.A. **Competing interests:** The authors declare that they have no competing interests. **Data and materials availability:** All data needed to evaluate the conclusions in the paper are present in the paper and/or the Supplementary Materials. Additional data related to this paper may be requested from the authors.

Submitted 30 July 2018
Accepted 24 September 2018
Published 31 October 2018
10.1126/sciadv.aau9483

**Citation:** T. M. Smith, C. Austin, D. R. Green, R. Joannes-Boyau, S. Bailey, D. Dumitriu, S. Fallon, R. Grün, H. F. James, M.-H. Moncel, I. S. Williams, R. Wood, M. Arora, Wintertime stress, nursing, and lead exposure in Neanderthal children. *Sci. Adv.* **4**, eaau9483 (2018).

# Wintertime stress, nursing, and lead exposure in Neanderthal children

Tanya M. Smith, Christine Austin, Daniel R. Green, Renaud Joannes-Boyau, Shara Bailey, Dani Dumitriu, Stewart Fallon, Rainer Grün, Hannah F. James, Marie-Hélène Moncel, Ian S. Williams, Rachel Wood and Manish Arora

*Sci Adv* **4** (10), eaau9483.
DOI: 10.1126/sciadv.aau9483